Computational Mechanics of a Coupled Flow-Structure Interaction Problem with Applications to Bio-inspired Micro Air Vehicles

*Rohan Banerjee[1], *Padmanabhan Seshaiyer[2]

[1]Thomas Jefferson High School for Science and Technology, Alexandria, VA 22312, USA
[2]Mathematical Sciences, George Mason University, Fairfax, VA 22030, USA

*Corresponding authors: rohan.b.banerjee@gmail.com, pseshaiy@gmu.edu

Abstract

Micro Air Vehicles (MAVs) are small flying vehicles that are designed to fit certain size and weight constraints. MAVs are important because they have a variety of practical applications, including surveillance and weather imaging. MAVs fall into two major categories according to their lift mechanism, either fixed-wing or flapping-wing, and wing structure, either rigid or flexible. Much research has been devoted to fixed wing, flexible MAVs consisting of rigid stabilizing battens and a rigid central fuselage coupled with a flexible membrane. We used finite element software to implement a system of PDEs that represented the MAV wing. The goal of this study was to computationally verify qualitative results showing that varying the number of stabilizing battens and the angle of attack affected the wing deformation. The work will be extended to include rigorous stability estimates, which will provide a better understanding of flexible wing MAV aerodynamics, and nonlinear membrane models.

Keywords: Micro Air Vehicles, multiphysics, mechanics, PDE, finite element method

Introduction

Applications in computational mechanics have expanded with the need to solve sophisticated fluid-structure applications using novel computational methodologies. Solving these coupled systems efficiently helps to understand complex non-linear interactions that arise in several applications such as blood flow interaction with arterial wall (Bathe and Kamm, 1999; Nobile, 2001) and computational aeroelasticity of flexible wing flying vehicles (Ferguson, 2006), where the structural deformation and flow field interact in a highly complex way. This study focuses specifically on the applications of computational mechanics to flexible-wing MAVs.

Micro Air Vehicles (MAVs) are small, autonomous flying vehicles which are designed for use in applications where human intervention would be either costly or dangerous. MAVs have the potential to be used in a large number of applications, including military reconnaissance and weather imaging. A number of variations on MAVs have been considered in computational and experimental studies. One type of MAV is the flexible-wing MAV, in which a flexible membrane is attached to a rigid body, allowing the wing to passively deform during the course of a flight. The other major type of MAV is the biologically-inspired flapping-wing MAV. A number of studies have been conducted which examine the thrust performance of flapping-wing mechanisms (La Mantia and Dabnichki, 2013). Unfortunately, constructing flapping-wing MAVs that satisfy power and stability requirements is often very difficult (Ifju et. al, 2002). Therefore, in this study, we computationally modeled the behavior of a particular variant of the flexible-wing MAV designed and tested by Ifju, et al.
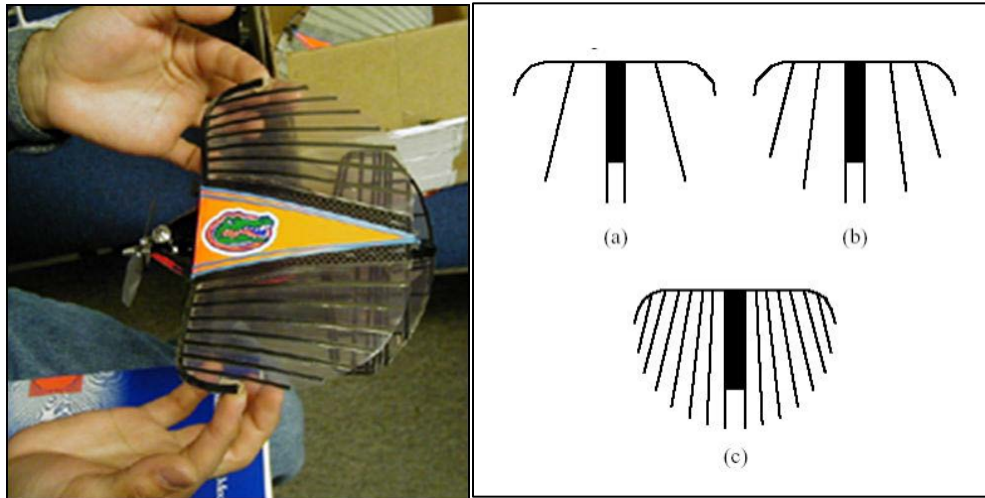
Figure 1. Flexible Wing MAV Model: (Left) 7-batten flexible wing MAV developed by the University of Florida (Ifju et. al, 2002); (Right) Schematic of one-batten (a), two-batten (b), and six-batten (c) flexible wing MAV designs (Ifju et. al, 2002)

The Micro Air Vehicles developed by Ifju, et al. consist of a rigid skeleton consisting of a central fuselage and stabilizing battens which run perpendicular to the fuselage. Superimposed upon this rigid skeleton is a flexible membrane, typically constructed out of an extensible latex rubber membrane or an inextensible monofilm membrane. A number of different wings were theorized and tested by Ifju, of which the designs of note are displayed in Figure 1. In addition, Ifju et al. have conducted experimental studies that indicate the influence of the number of battens on the lift performance in relation to varying angles of attack (see Figure 2).
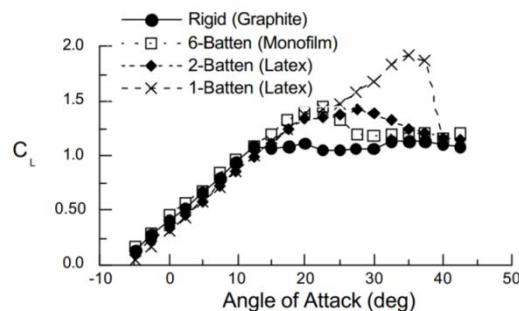

Figure 2. Lift Coefficient vs. Angle of Attack for various MAV configurations (Ifju, et al)

The major difference between the different designs is the number of stabilizing battens used, in addition to the type of membrane. One of the qualitative conclusions of the aforementioned study was that increasing the number of battens generally resulted in stiffer designs that exhibited smaller magnitudes of membrane vibration and deformation. The goal of this study was to computationally verify these qualitative experimental results and examine the role of the angle of attack on the membrane deflection.

Models, Methods, and Governing Differential Equations

Model Problem

In order to mathematically model the wing of the flexible-wing MAV, we first formulated a simplified geometry from which we subsequently imposed a system of partial differential equations. The geometry consisted of a 2D elliptical surface describing the underlying membrane, with 2D rectangles superimposed upon the ellipse which represented both the stabilizing battens and the central fuselage. The wing surface was superimposed on the face of a 3D cylinder, which represented a wind tunnel through which air could flow. The cylinder could be inclined to simulate different angles of attack, which describe at what angle the airflow makes contact with the MAV surface. A schematic showing the geometry and the different domains and boundaries of interest is shown in Figure 3.
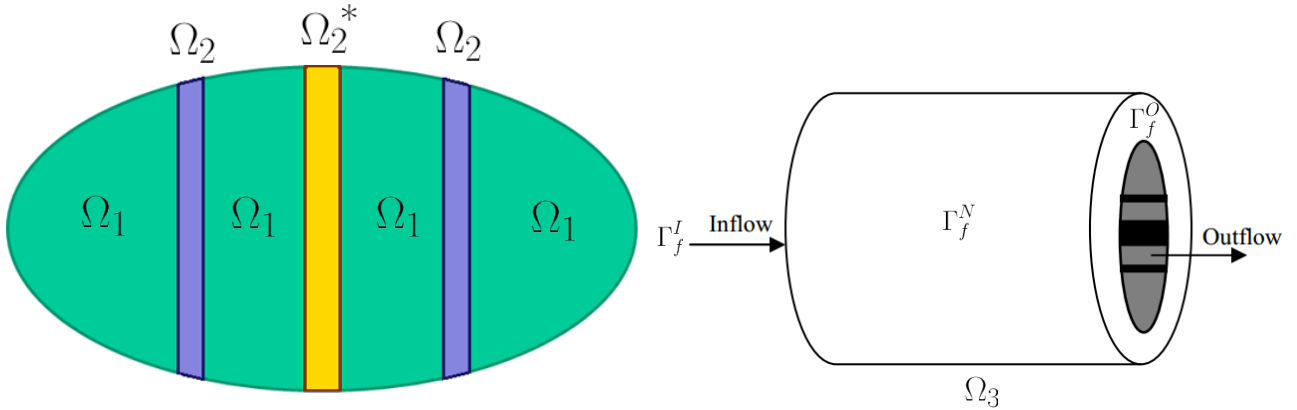
Figure 3. Subdomains of the wing structure for 1-batten MAV (top), schematic of airflow and 1-batten MAV wing placement (Nong et al., 2010) (bottom)

In Figure 3, Note that Ω_1 represents the flexible membrane, Ω_2 represents the battens, and Ω_2^* represents the fuselage (which differs from the battens only in elastic modulus). In addition, Ω_3 represents the entire 3D fluid domain, Γ_f^I represents the inflow face of the cylinder, Γ_f^N represents the rectangular outer face of the cylinder, and Γ_f^O represents the outflow face of the cylinder, not including the region where the MAV is placed.

Governing PDE System

We modeled the deformation of the flexible membrane using a linear elastic membrane model based on Hooke's Law. This led to a PDE for the membrane which involved w, the transverse displacement of the membrane in space and time, shown below:

$$\rho_{s0} \frac{\partial^2 w}{\partial t^2} - E_0 \nabla^2 w = p \text{ (in } \Omega_1) \tag{1}$$

Note in equation 1 that the right hand side represents the fluid pressure, to be defined later. To model the stabilizing beams, we used Euler-Bernoulli beam theory, which gives another PDE involving w.

Adding the Euler-Bernoulli beam equation to the prior membrane equation yields the following set of PDEs (Nong et al., 2010):

$$(\rho_{s0} + \rho_{s1})\frac{\partial^2 w}{\partial t^2} - E_0 \nabla^2 w + E_1 \frac{\partial^2 v}{\partial y^2} = p \text{ (in } \Omega_2)$$
$$v = \frac{\partial^2 w}{\partial y^2} + \epsilon \nabla^2 v \text{ (in } \Omega_1 \cup \Omega_2)$$

(2)

Note the presence of an additional dependent variable v, which is an auxiliary variable used to facilitate the computational simulation of the system. The fuselage (Ω_2^*) satisfies in identical system of PDEs, only differing in the values of certain constants as previously mentioned.

We assumed that the fluid flow was incompressible, irrotational, and inviscid, allowing us to use the potential flow model for our airflow. This involved the introduction the velocity potential ϕ, satisfying Laplace's equation:

$$\nabla^2 \phi = 0 \text{ (in } \Omega_3)$$

(3)

The fluid pressure is defined according to Bernoulli's Equation for flow, which relates the fluid velocity, density, pressure, and transverse displacement as follows:

$$p = -\rho_f \phi_t - \rho_f g w$$

(4)

PDE Boundary Conditions

We imposed certain boundary conditions on the MAV wing model and the wind tunnel cylinder to simulate realistic constraints. The bottom half of the MAV wing employed a Dirichlet boundary constraint to simulate a fixed, rigid beam, while the upper half of the MAV wing employed a Neumann boundary constraint to represent the free membrane, as follows:

$$w = 0 \text{ (on lower boundary)}$$
$$\vec{n} \cdot \nabla w = 0 \text{ (on upper boundary)}$$

(5)

The inflow boundary condition for the fluid domain was specified by stating a constant value for the normal component of the fluid velocity on the inflow face. The normal fluid velocity on the outer, rectangular boundary of the cylinder was set to 0. The outflow boundary condition was specified using Sommerfeld's radiation condition (Schot, 1992), which relates the normal fluid velocity on the right face of the cylinder to the time partial derivative of the velocity potential. The boundary conditions for the cylinder are described in Equation 6:

$$\nabla \phi \cdot \vec{n} = 0 \text{ (on } \Gamma_f^N)$$
$$\nabla \phi \cdot \vec{n} = -c \text{ (on } \Gamma_f^I)$$
$$\nabla \phi \cdot \vec{n} = -\alpha \frac{\partial \phi}{\partial t} \text{ (on } \Gamma_f^O)$$

(6)

Table 1 contains the parameter values used in our model (all non-cited values are either fundamental constants or are defined by the authors):

Table 1. Parameter Values

Variable	Value
Density of Membrane (ρ_{s0})	$10 \ \text{kg} \cdot \text{m}^{-3}$
Density of Beams (ρ_{s1})	$100 \ \text{kg} \cdot \text{m}^{-3}$
Density of Air (ρ_f)	$1.293 \ \text{kg} \cdot \text{m}^{-3}$ (Nave, 1999)
Young's Modulus Factor for Membrane (E_0)	$1 \ \text{N} \cdot \text{m}^{-1}$
Young's Modulus Factor for Beams (E_1)	$10 \ \text{N} \cdot \text{m}$
Young's Modulus Factor for Fuselage (E_3)	$1000 \ \text{N} \cdot \text{m}$
Smoothing Factor (ϵ)	$10^{-5} \ \text{m}$
Acceleration of gravity (g)	$9.8 \ \text{m} \cdot \text{s}^{-2}$
Inflow velocity (c)	$0.1 \ \text{m} \cdot \text{s}^{-1}$
Sommerfeld Radiation Constant (α)	$50 \ \text{s} \cdot \text{m}^{-1}$

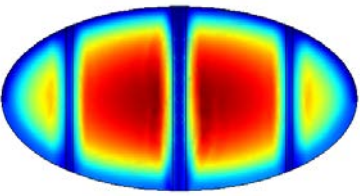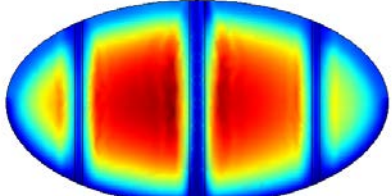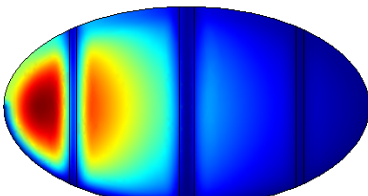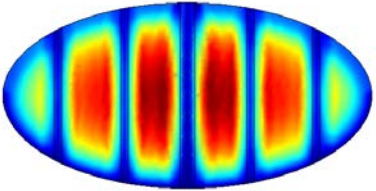## Computational Results
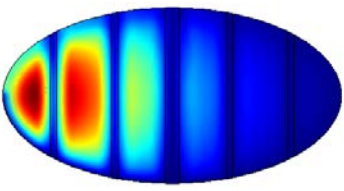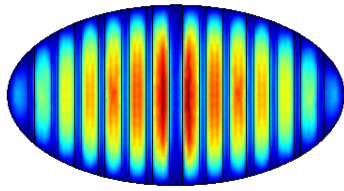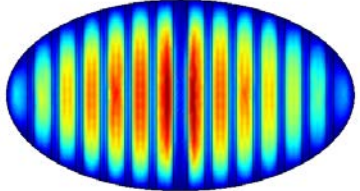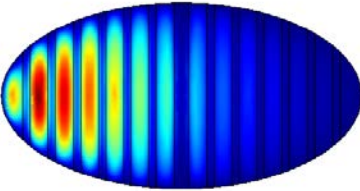
Solution Methodology
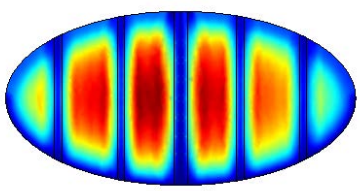
We then implemented computationally the PDE system described in Equations 1-4 and the boundary conditions described in Equations 5-6 using the finite element method. Specifically, we discretized Equations 1-4 and developed the weak formulation of the governing differential equations for the flow and the structure. These were coupled through interface variables that matched the velocity of the flow to the time derivative of the transverse displacement of the membrane-beam model.

This algorithm was implemented using the multiphysics software COMSOL. The software utilized a backward Euler scheme in time and used the UMFPACK (Unsymmetric Multifrontal Sparse LU Factorization Package) for solving the resulting linear systems. The geometry was discretized using triangular and tetrahedral elements.

Results

We conducted numerical simulations with the three batten configurations shown in Figure 1, consisting of one-batten, two-batten, and six-batten wing skeletons. Additionally, we investigated three different angles of attack for the fluid, namely 90$^\text{o}$, 80$^\text{o}$, and 15$^\text{o}$. We investigated the nine possible fluid-structure combinations and we have reproduced the results in the table below, showing the deflection of the MAV membrane at $t = 1$ for varying numbers of battens and angles of attack as well as the maximum deflection of the MAV wing:

Table 2. Numerical Results

	90 degrees	80 degrees	15 degrees
1-batten	Maximum deflection: 0.0213	Maximum deflection: 0.0217	Maximum deflection: 0.0161
2-batten	Maximum deflection: 0.0218	Maximum deflection: 0.0138	Maximum deflection: 0.0164
6-batten	Maximum deflection: 0.0165	Maximum deflection: 0.0161	Maximum deflection: 0.0096

Upon inspection of Table 2, there are two general trends of note. The first is that proceeding from top to bottom in each column of the matrix, which corresponds to increasing the number of battens while fixing the angle of attack, results in a general decrease in the maximum deflection of the MAV wing, with some irregularities. This seems to confirm the qualitative observations of Ifju et al., which stated that increasing the number of battens would increase the rigidity of the wing.

The second trend is that when proceeding from left to right in each row of the matrix, which corresponds to decreasing the angle of attack while fixing the number of battens, the maximum deflection also tends to decrease. Again, there are some irregularities, but overall this seems to confirm the expectation that lowering the angle of attack would decrease the maximum displacement. This presumably occurs because with smaller angles of attack, the normal component of the velocity is reduced, thus reducing the magnitude of the fluid pressure and therefore the magnitude of the deformation.

In order to gain another perspective on the deformation profile of the flexible wing MAVs, we have created the following set of graphs, shown in Figure 4:

(a)   **(b)**

(c)
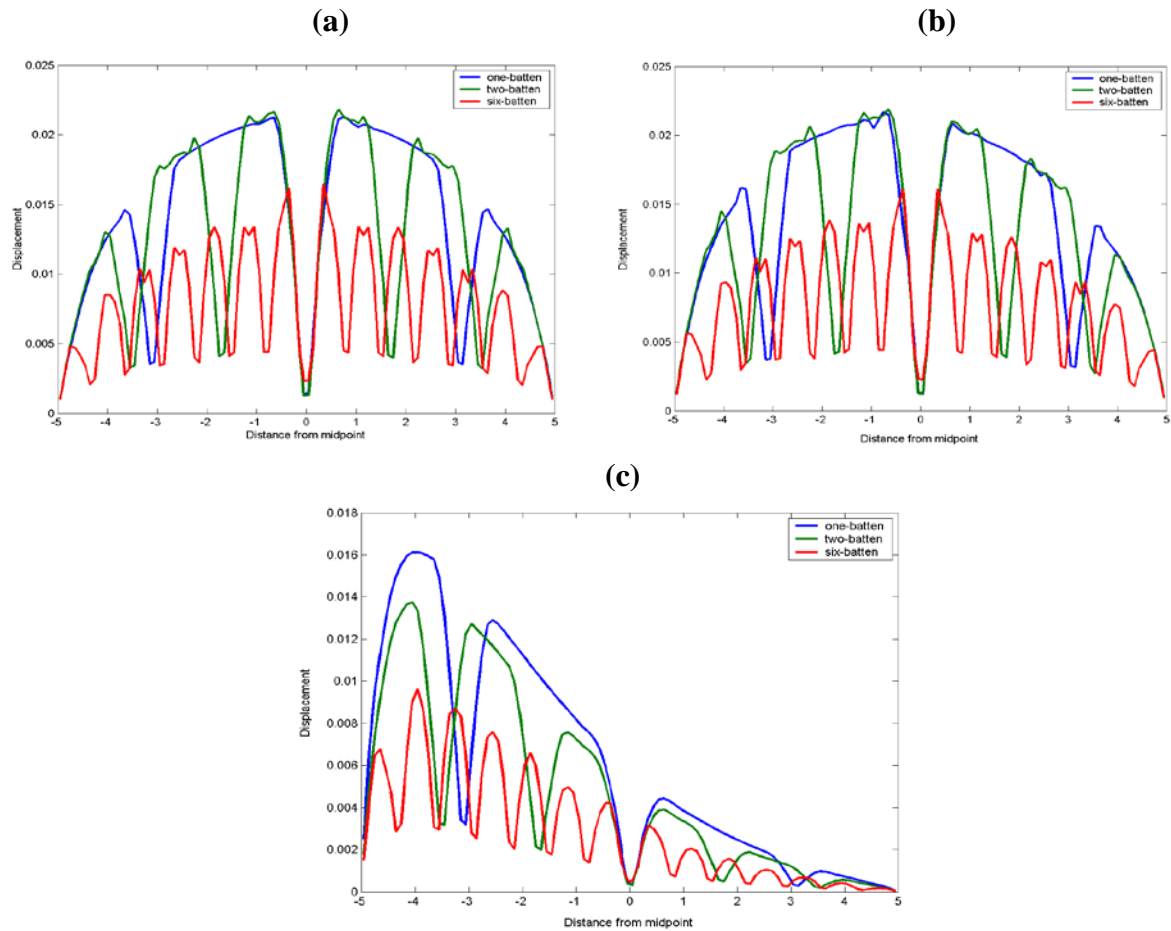
Figure 4. The effect of varying the number of battens on the deformation of the MAV wing for angle of attack 90° (a), 80° (b), 15° (c)

The graphs in Figure 4 show the one-batten configurations in blue, the two-batten configurations in green, and the six-batten configurations in red. The graphs confirm that increasing the number of battens reduces the overall deformation, but they also reveal an interesting result: changing the number of battens from one to two actually increases the overall deformation slightly for the 90° and 80° angle-of-attack scenarios. The graphs also confirm the aforementioned observations about the angle of attack.

Conclusion and Future Directions

In this paper, we have implemented the mathematical model initially investigated by Nong, et al, consisting of a PDE system that is meant to model the deformation of a flexible-wing MAV with multiple battens. We have been able to generally verify the qualitative observations made by Ifju, et al about the effect of altering the number of battens on wing deformation, with some exceptions.

Additionally, we have shown that decreasing the angle of attack of the MAV wing decreases the observed maximum deformation.

There are a number of potential future directions for this research. The first is to computationally validate the quantitative experimental results derived by Ifju, et al dealing with the coefficient of lift, which were shown in Figure 2. The tests to computationally verify Figure 2 will be done through a joint use of the COMSOL multiphysics software and a separate fluid dynamics package. Other modifications involve changing the material properties of the MAV wing to produce material non-linearity, which include considering non-linear elastic membrane models. Geometric non-linearity in the membrane and beam models will potentially be incorporated. Finally, a rigorous stability analysis for the coupled Fluid-Structure Interaction problem will be performed. This will involve a more complex model for the membrane which accounts for both axial (in-plane) and transverse displacements and will be based on establishing bounds for the mechanical energy of the MAV wing.

References

Bathe, M. and Kamm, R.D. (1999), A Fluid-Structure Interaction Finite Element Analysis of Pulsatile Blood Flow Through a Compliant Stenotic Artery. *Journal of Biomechanical Engineering*, 121, pp. 361–369.

Ferguson, L. (2006), A computational model for flexible wing based micro air vehicles. Master's Thesis, Texas Tech University.

Ifju, P.G., Jenkins, D.A., Ettinger, S., Lian, Y., & Shyy, W. (2002), Flexible-wing-based micro air vehicles. *American Institute of Aeronautics & Astronautics*, pp. 1-13.

La Mantia, M., & Dabnichki, P. (2013), Structural response of oscillating foil in water. *Engineering Analysis with Boundary Elements*, *37*(6), pp. 957-966.

Nave, C. R. (1999), Densities of common substances. Retrieved from Hyperphysics: Department of Physics and Astronomy website: http://hyperphysics.phy-astr.gsu.edu/hbase/tables/density.html

Nobile, F. (2001), Numerical approximation of fluid-structure interaction problems with application to haemodynamics, Ph.D. Thesis, EPFL, Lausanne.

Nong, K., Aulisa, E., Garcia, S., Swim, E., & Seshaiyer, P. (2010), Computational methods for multi-physics applications with fluid-structure interaction. *Proceedings of the COMSOL Conference Boston*, 1-5.

Schot, S.H. (1992). Eighty Years of Sommerfeld's Radiation Condition. *HISTORIA MATHEMATICA,* 19 (4), pp. 385-401.